Dynamical evolutions of ℓ-boson stars in spherical symmetry

Miguel Alcubierre,[1] Juan Barranco,[2] Argelia Bernal,[2] Juan Carlos Degollado,[3]
Alberto Diez-Tejedor,[2] Miguel Megevand,[4] Darío Núñez,[1] and Olivier Sarbach[5]

[1]*Instituto de Ciencias Nucleares, Universidad Nacional Autónoma de México,*
Circuito Exterior C.U., A.P. 70-543, México D.F. 04510, México
[2]*Departamento de Física, División de Ciencias e Ingenierías,*
Campus León, Universidad de Guanajuato, León 37150, México
[3]*Instituto de Ciencias Físicas, Universidad Nacional Autónoma de México,*
Apdo. Postal 48-3, 62251, Cuernavaca, Morelos, México
[4]*Instituto de Física Enrique Gaviola, CONICET. Ciudad Universitaria, 5000 Córdoba, Argentina*
[5]*Instituto de Física y Matemáticas, Universidad Michoacana de San Nicolás de Hidalgo,*
Edificio C-3, Ciudad Universitaria, 58040 Morelia, Michoacán, México
(Dated: October 10, 2019)

In previous work, we have found new static, spherically symmetric boson star solutions which generalize the standard boson stars by allowing a particular superposition of scalar fields in which each of the fields is characterized by a fixed value of its non-vanishing angular momentum number ℓ. We call such solutions "ℓ-boson stars". Here, we perform a series of fully non-linear dynamical simulations of perturbed ℓ-boson stars in order to study their stability, and the final fate of unstable configurations. We show that for each value of ℓ, the configuration of maximum mass separates the parameter space into stable and unstable regions. Stable configurations, when perturbed, oscillate around the unperturbed solution and very slowly return to a stationary configuration. Unstable configurations, in contrast, can have three different final states: collapse to a black hole, migration to the stable branch, or explosion (dissipation) to infinity. Just as it happens with $\ell = 0$ boson stars, migration to the stable branch or dissipation to infinity depends on the sign of the total binding energy of the star: bound unstable stars collapse to black holes or migrate to the stable branch, whereas unbound unstable stars either collapse to a black hole or explode to infinity. Thus, the parameter ℓ allows us to construct a new set of stable configurations. All our simulations are performed in spherical symmetry, leaving a more detailed stability analysis including non-spherical perturbations for future work.

PACS numbers: 04.20.q, 04.25.Dm, 95.30.Sf, 98.80.Jk

I. INTRODUCTION

Scalar fields are an ubiquitous theme in modern cosmology [1–5]. They can also form localized, globally regular, self-gravitating configurations. Depending on the scalar field properties, different types of configurations have been found such as oscillatons [6] (for real scalar fields), boson stars (BSs) [7, 8], BSs with self-interaction [9], multistate BSs [10], and multi-oscillating BSs [11]. Further studies have shown that BS's may also have electric charge and/or rotation. Since then many works have been dedicated to study their nature and their potential detection as BHs mimickers (see [12, 13] for reviews).

For some values of the mass of the constituent boson, BSs are indistinguishable from BHs in the weak field region. For this reason, BSs have been considered as alternatives for the central galactic BHs [14–16]. It is then important to be able to differentiate between the two objects, which can both account for current observable constraints. Despite the fact that recent observations of the center of the galaxy M87 by the Event Horizon Telescope [17] have already put important constraints on black hole alternatives (including BSs [18, 19]), there is still a need to better understand their physical properties to accurately model their associated accretion flow and

resulting image.

Recently we have found new BS solutions that we have called ℓ-boson stars [20].[1] These ℓ-boson stars are compact spherically symmetric configurations composed by an odd number of complex scalar fields. The configurations are parametrized by an angular momentum number ℓ, hence the name, with the $\ell = 0$ case corresponding to the standard well-known boson stars. In particular, ℓ-boson stars can be extremely compact objects, approaching the Buchdahl limit[2] $M/R < 4/9 \sim 0.44$ (for $\ell = 4$ we

---

[1] We have recently become aware of related work by Mielke and Scherzer in 1981 [21], where similar configurations of the Einstein-Klein-Gordon system are studied. In their work, they also consider families of complex scalar fields. However, their procedure involves an averaging of the stress-energy tensor over the sphere in order to get rid of the angular dependency, whereas in our work the family is deliberately chosen such that the angular dependency is exactly cancelled in the total stress-energy tensor without taking averages. We thank E. Mielke for pointing Ref. [21] to us.

[2] See Ref. [22] for a rather general result regarding the Buchdahl limit and generalizations thereof for static, spherically symmetric spacetimes. Interestingly, the ℓ-boson stars discussed in this article *do not* satisfy the assumption of a non-negative radial pressure made in that reference.

have found solutions with $M/R \sim 0.3$).

Any astrophysical model for a compact object, in order to be viable, must be stable or at least stable for a sufficiently long time. In this work we therefore focus on studying the stability properties of ℓ-boson stars. In order to test the nonlinear (in)stability of these solutions we perform fully nonlinear numerical simulations in spherical symmetry. We use as initial data the configurations found in [20], and perturb them in several ways, namely adding or subtracting a small quantity of mass while trying to keep the total number of particles fixed. We have found that stable configurations, when perturbed, oscillate around the unperturbed solution and seem to very slowly return to a stationary configuration. Unstable configurations, in contrast, can have three different final states: collapse to a black hole, migration to the stable branch, or explosion (dissipation) to infinity. Just as it happens with $\ell = 0$ boson stars, migration to the stable branch or dissipation to infinity depend on the sign of the total binding energy of the star: bound unstable stars collapse to black holes or migrate to the stable branch, whereas unbound unstable stars either collapse to a black hole or explode to infinity. It is important to mention that for both stable configurations, and unstable configurations that migrate to the stable branch, the relaxation times seem to be extremely long. In some cases we have followed these configurations for thousands of light crossing times (millions of numerical time steps) and, although we can be quite confident that the final state is indeed stable, at this point we can not rule out the possibility that those configurations will not settle down to a single frequency ℓ-boson star, but will settle instead to some form of multi-oscillating solution such as those recently studied in [11].

The paper is organized as follows: In Section II we describe the Einstein Klein-Gordon system and the decomposition of the fields required to have a spherically symmetric configuration. In Section III we review the stationary solutions found in [20] that are used as initial data in our numerical evolutions. In Section IV we give a description of the type of perturbations we apply to the static solutions. In Section V we present the analysis tools and numerical techniques used in our simulations. We present our results in section VI. Finally, in Section VII we give some concluding remarks.

II.   THE EINSTEIN KLEIN-GORDON SYSTEM

We will consider a collection of an arbitrary odd number of complex, non-interacting scalar fields of equal mass μ, minimally coupled to gravity. Following [20, 23] we consider solutions of the form

$$\Phi_{\ell m}(t, r, \vartheta, \varphi) = \phi_\ell(t, r) Y^{\ell m}(\vartheta, \varphi), \qquad (1)$$

where the angular momentum number ℓ is fixed, and m takes values $m = -\ell, -\ell+1, \ldots, \ell$. As usual $Y^{\ell m}$ denotes the standard spherical harmonics, and the amplitudes

$\phi_\ell(t, r)$ are the *same* for all m. As already shown in [20, 23], this leads to a total stress energy-momentum tensor which is spherically symmetric.

In order to solve the field equations, we will then consider a spherically symmetric spacetime with a line element given by:

$$ds^2 = -\alpha^2 dt^2 + \psi^4 \left(A dr^2 + r^2 B d\Omega^2 \right) , \qquad (2)$$

where (α, A, B, ψ) are functions of (r, t) only, and $d\Omega^2$ is the standard solid angle element. Notice that this form of the metric might seem too generic, and in order to find boson star initial data one typically takes $\psi = B = 1$. [3] However, this is the form of the metric we will use for our dynamical simulations below, since we will be using a spherically symmetric version of the Baumgarte-Shapiro-Shibata-Nakamura (BSSN) formulation [24–27]. With these assumptions and definitions, the Klein-Gordon equation can be written in first order form as (for simplicity we will suppress the index ℓ):

$$\partial_t \phi = \alpha \Pi , \qquad (3)$$
$$\partial_t \chi = \alpha \partial_r \Pi + \Pi \partial_r \alpha , \qquad (4)$$
$$\partial_t \Pi = \frac{\alpha}{A\psi^4} \left[\partial_r \chi + \chi \left(\frac{2}{r} - \frac{\partial_r A}{2A} + \frac{\partial_r B}{B} + 2\,\partial_r \psi \right) \right]$$
$$+ \frac{\chi \, \partial_r \alpha}{A\psi^4} + \alpha K \Pi - \alpha \left(\mu^2 + \frac{\ell(\ell+1)}{r^2 B \psi^4} \right) , \qquad (5)$$

with $K = K_m^m$ the trace of the extrinsic curvature of the hypersurfaces of constant time, and where we have defined: [4]

$$\chi := \partial_r \phi , \qquad \Pi := \frac{\partial_t \phi}{\alpha} . \qquad (6)$$

Furthermore, the stress-energy tensor can be shown to take the form [20]:

$$T_{mn} = (\partial_m \phi)^*(\partial_n \phi) - \frac{\gamma_{mn}}{2} \left[\gamma^{pq}(\partial_p \phi)^*(\partial_q \phi) \right.$$
$$\left. + \left(\mu^2 + \frac{\ell(\ell+1)}{r^2} \right) |\phi|^2 \right] ,$$
$$T_{mN} = 0 , \qquad (7)$$
$$T_{MN} = -r^2 B \psi^4 \frac{\gamma_{MN}}{2} \left[\gamma^{pq} \left(\partial_p \phi \right)^* \left(\partial_q \phi \right) + \mu^2 |\phi|^2 \right] ,$$

where here $(m, n) = (t, r)$, $(M, N) = (\vartheta, \varphi)$, γ_{mn} is the 2D time–radial metric, $\gamma_{mn} dx^m dx^n = -\alpha^2 dt^2 + A\psi^4 dr^2$, and γ_{MN} the 2D angular metric for the unit sphere, $\gamma_{MN} dx^M dx^N = d\Omega^2$.

Notice that the normalization in the above expressions for the stress-energy tensor differs from the one used in

---

[3] Note that the form of the metric used here differs from the one of Ref. [20]. In particular, in that reference we used $\psi = B = 1$, and $\gamma = \sqrt{A}$.

[4] Again, note that the definition of χ in Eq. (6) differs from the definition of the quantity χ_ℓ in [20] by a factor of $\gamma = \sqrt{A}$.

reference [20] by a factor of $(2\ell + 1)/4\pi$. The reason for this is that we have absorbed that factor into the definition of ϕ in order to be consistent with the normalization used in the numerical evolution code, which takes ϕ as a single scalar field with a modified evolution equation and stress-energy tensor, instead of a sum over $(2\ell + 1)$ independent fields (the extra factor of 4π comes from the normalization of the spherical harmonics). With the normalization above the Einstein field equations take the standard form $G_{\mu\nu} = 8\pi T_{\mu\nu}$ (we use Planck units such that $G = c = \hbar = 1$).

With the expressions above for the stress-energy tensor, the energy density ρ_E, momentum density P_i and stress tensor S_{ij} as seen by the normal (Eulerian) observers become:

$$\rho_E = n^\mu n^\nu T_{\mu\nu}$$
$$= \frac{1}{2}\left[|\Pi|^2 + \frac{|\chi|^2}{A\psi^4} + \left(\mu^2 + \frac{\ell(\ell+1)}{r^2}\right)|\phi|^2\right], \quad (8)$$

$$P_r = -n^\mu T_{r\mu} = -\frac{1}{2}(\chi\Pi^* + \Pi\chi^*), \quad (9)$$

$$S_r^r = \frac{1}{2}\left[|\Pi|^2 + \frac{|\chi|^2}{A\psi^4} - \left(\mu^2 + \frac{\ell(\ell+1)}{r^2}\right)|\phi|^2\right], \quad (10)$$

$$S_\theta^\theta = \frac{1}{2}\left[|\Pi|^2 - \frac{|\chi|^2}{A\psi^4} - \mu^2|\phi|^2\right], \quad (11)$$

where $n^\mu = (1/\alpha, 0, 0, 0)$ is the unit normal vector to the spatial hypersurfaces. In particular, the momentum density is purely radial because of the spherical symmetry.

III. STATIONARY INITIAL DATA

We will consider stationary ℓ-boson stars, with a complex scalar field that has the form:

$$\phi(r, t) = \varphi(r)e^{i\omega t}, \quad (12)$$

with ω and $\varphi(r)$ real-valued. At $t = 0$ this implies:

$$\phi(r, t = 0) = \varphi, \quad (13)$$
$$\chi(r, t = 0) = \varphi', \quad (14)$$
$$\Pi(r, t = 0) = i\omega\varphi/\alpha. \quad (15)$$

We then see that the initial scalar field and its radial derivative are purely real, while the initial time derivative is purely imaginary.

The initial data for stationary ℓ-boson stars was discussed in detail in [20]. As discussed there, even though the scalar field oscillates in time the stress-energy tensor is time-independent, and these objects result in static solutions to the Einstein field equations. In order to find initial data, one substitutes the ansatz (12) in the Klein-Gordon equation, assumes that the spatial metric is in the areal gauge so that $\psi = B = 1$ in the metric (2) above, asks for the spacetime metric to be static so that the extrinsic curvature K_{ij} vanishes, and solves

the Hamiltonian constraint for the radial metric A. For the lapse function α we use the "polar slicing" condition, which asks for the time derivative of the angular component of the extrinsic curvature to vanish, $\partial_t K_{\theta\theta} = 0$, and results in a first order differential equation for the lapse function α. This results in the following system of three equations (Klein-Gordon equation, Hamiltonian constraint and polar slicing condition respectively):

$$\partial_r^2 \varphi = -\partial_r\varphi\left(\frac{2}{r} + \frac{\partial_r\alpha}{\alpha} - \frac{\partial_r A}{2A}\right)$$
$$+ A\varphi\left(\mu^2 + \frac{\ell(\ell+1)}{r^2} - \frac{\omega^2}{\alpha^2}\right), \quad (16)$$

$$\partial_r A = A\left\{\frac{(1-A)}{r} + 4\pi r A\left[\frac{(\varphi')^2}{A}\right.\right.$$
$$+ \left.\left.\varphi^2\left(\mu^2 + \frac{\ell(\ell+1)}{r^2} + \frac{\omega^2}{\alpha^2}\right)\right]\right\}, \quad (17)$$

$$\partial_r\alpha = \alpha\left[\frac{(A-1)}{r} + \frac{\partial_r A}{2A}\right.$$
$$- \left.4\pi r A\varphi^2\left(\mu^2 + \frac{\ell(\ell+1)}{r^2}\right)\right]. \quad (18)$$

Notice that instead of polar slicing one could ask for a maximal slicing condition, $\partial_t K = 0$, which in this case can be shown to be equivalent, but results in a second order differential equation for α instead.

By analyzing the Klein-Gordon equation one finds that for small r the scalar field behaves as $\varphi \sim \varphi_0 r^\ell$. For a fixed value of ℓ, and a given value of the parameter φ_0, the above system of equations becomes a nonlinear eigenvalue problem for the frequency ω, subject to the boundary condition that φ decays exponentially far away.

In [20] it was also found that ℓ-boson stars possess similar properties to those of standard $\ell = 0$ boson stars. Specifically, for a given angular momentum number ℓ, as the parameter φ_0 increases, the equilibrium configurations exhibit a maximum value of the mass, and this maximum grows with ℓ, leading to more compact objects. Also, for each value of ℓ, the space of solutions separates in two distinct branches to either side of the maximum mass. We will show below that, just as occurs with the $\ell = 0$ case, those two branches correspond to stable and unstable configurations.

Before introducing perturbations to the initial data for the ℓ-boson stars, it is important to consider three physical quantities related to the scalar field that are important in characterizing the different solutions. The first two are the energy density ρ_E (given by equation (8) above), and the boson (particle) density ρ_B:

$$\rho_E = \frac{1}{2}\left[|\Pi|^2 + \frac{|\chi|^2}{A\psi^4} + \left(\mu^2 + \frac{\ell(\ell+1)}{r^2}\right)|\phi|^2\right], \quad (19)$$

$$\rho_B = -n^\mu J_\mu = \phi_R\Pi_I - \phi_I\Pi_R, \quad (20)$$

where J^μ is the conserved particle current

$$J^\mu = -\frac{1}{2}\text{Im}(\phi^*\nabla^\mu\phi - \phi\nabla^\mu\phi^*), \quad (21)$$

and where the sub-indices R and I refer to the real and imaginary parts respectively. Substituting the ansatz (12) these expressions reduce to:

$$\rho_E = \frac{1}{2}\left[\frac{(\varphi')^2}{A\psi^4} + \left(\mu^2 + \frac{\ell(\ell+1)}{r^2} + \frac{\omega^2}{\alpha^2}\right)\varphi^2\right], \quad (22)$$

$$\rho_B = \omega\varphi^2/\alpha. \quad (23)$$

Notice that both these quantities are clearly time independent.

The third quantity we need to consider is the momentum density of the scalar field, which is given by equation (9) above, and has the form:

$$P_r = -\frac{1}{2}\left(\chi\Pi^* + \Pi\chi^*\right) = -\chi_R\Pi_R - \chi_I\Pi_I. \quad (24)$$

This can now be easily shown to vanish when we substitute the ansatz (12). Notice that, since the spacetime metric for the ℓ-boson stars is static and the momentum density vanishes, the momentum constraint is trivially satisfied and can be safely ignored when solving for the initial data.

IV. PERTURBED INITIAL DATA

We will now add to the stationary initial data described above small (but non-linear) perturbations, such that at $t = 0$ we will have:

$$\phi_R = \varphi_0 + \delta\varphi_R, \qquad \phi_I = \delta\varphi_I, \quad (25)$$
$$\Pi_R = \delta\Pi_R, \qquad \Pi_I = (\Pi_I)_0 + \delta\Pi_I, \quad (26)$$

where the subindex 0 refers to the unperturbed solution. Notice that in particular we have $(\Pi_I)_0 = \omega\varphi_0/\alpha_0$, with α_0 the unperturbed lapse and ω the frequency of the unperturbed solution.

We will consider first the effect that this perturbation has on the momentum density. The reason for this is that the initial data, once perturbed, will not correspond any more to a static spacetime. However, for simplicity, we would like to ask for the initial data to be time symmetric, so that we can still ignore the momentum constraint and only solve the Hamiltonian constraint at $t = 0$. But in order to do this we must ask for the perturbation to keep the initial momentum density of the scalar field equal to zero.

Substituting the perturbation in the expression for the momentum density (24), and remembering that $\chi_{I,R} := \partial_r\varphi_{I,R}$, we find:

$$P_r = -\varphi_0'\delta\Pi_R - (\Pi_I)_0\delta\chi_I - \delta\Pi_R\delta\chi_R - \delta\Pi_I\delta\chi_I. \quad (27)$$

In order for P_r to vanish we must then ask for:

$$\varphi_0'\delta\Pi_R + (\Pi_I)_0\delta\chi_I + \delta\Pi_R\delta\chi_R + \delta\Pi_I\delta\chi_I = 0. \quad (28)$$

If we assume that the perturbations are small, we can ask for the linear and quadratic terms to vanish separately:

$$\varphi_0'\delta\Pi_R + (\Pi_I)_0\,\delta\chi_I = 0, \quad (29)$$
$$\delta\Pi_R\delta\chi_R + \delta\Pi_I\delta\chi_I = 0. \quad (30)$$

In principle there are may ways to satisfy these two conditions. The simplest choice is to ask for $\delta\Pi_R = \delta\varphi_I = \delta\chi_I = 0$, that is, the perturbation must be such that the initial value of ϕ (and hence χ) remains purely real, while the initial value of Π remains purely imaginary.

Consider now the boson density. The perturbed initial data will result in a boson density given by:

$$\rho_B = (\rho_B)_0 + \varphi_0\delta\Pi_I + (\Pi_I)_0\delta\varphi_R + \delta\varphi_R\delta\Pi_I - \delta\varphi_I\delta\Pi_R, \quad (31)$$

where $(\rho_B)_0$ is the unperturbed boson density given by (23). If we substitute the condition $\delta\Pi_R = \delta\varphi_I = 0$, this reduces to:

$$\rho_B = (\rho_B)_0 + \varphi_0\delta\Pi_I + (\Pi_I)_0\delta\varphi_R + \delta\varphi_R\delta\Pi_I. \quad (32)$$

Now, if we want a perturbation such that the boson density remains unchanged, we need to ask for:

$$\varphi_0\delta\Pi_I + (\Pi_I)_0\delta\varphi_R + \delta\varphi_R\delta\Pi_I = 0. \quad (33)$$

Again, for small perturbations we can ask for the linear and quadratic terms to vanish separately:

$$\varphi_0\delta\Pi_I + (\Pi_I)_0\delta\varphi_R = 0, \quad (34)$$
$$\delta\varphi_R\delta\Pi_I = 0. \quad (35)$$

We now immediately see that these two conditions can not both be satisfied at the same time unless both $\delta\varphi_R$ and $\delta\Pi_I$ vanish, so it is not possible to keep the boson density constant with these type of perturbations. However, for small perturbations we can still keep the linear part equal to zero in two special cases:

1. We choose an *external* perturbation, that is, one that has compact support outside the star, so that both $\phi_0\delta\Pi_I$ and $(\Pi_I)_0\delta\varphi_R$ will be identically zero. Notice that physically an external perturbation means that we are letting scalar field fall into the boson star from the outside. [5]

2. We choose an *internal* perturbation to the star such that:

$$\varphi_0\delta\Pi_I = -(\Pi_I)_0\delta\varphi_R. \quad (36)$$

Substituting now the value of $(\Pi_I)_0$ this conditon reduces to

$$\delta\Pi_I = -\frac{\omega}{\alpha_0}\delta\varphi_R. \quad (37)$$

---

[5] Boson stars in fact do not have a finite radius, so one can never have an "external" perturbation exactly. But the scalar field decays exponentially rapidly so we can have a very good approximation to this situation if the perturbation is sufficiently far away.

In both these cases, the perturbation will produce only a second order change in small quantities in the boson density $\delta\rho_B = \delta\varphi_R \delta\Pi_I$.

Finally, let us consider the effect of the perturbation in the energy density. We find:

$$
\begin{aligned}
\rho_E =\ & (\rho_E)_0 + Q(r)\varphi_0\delta\varphi_R + (\Pi_I)_0\delta\Pi_I + \frac{\varphi_0'\delta\chi_R}{A_0\psi_0^4} \\
& + \frac{1}{2}\left[\delta\Pi_R^2 + \delta\Pi_I^2 + \frac{1}{A_0\psi_0^4}\left(\delta\chi_R^2 + \delta\chi_I^2\right)\right. \\
& \left. + Q(r)\left(\delta\varphi_R^2 + \delta\varphi_I^2\right)\right] ,
\end{aligned}
\tag{38}
$$

with $(\rho_E)_0$ the unperturbed energy density give by (22), and where we introduced the shorthand $Q(r) := \mu^2 + \ell(\ell+1)/r^2$. If we take again $\delta\Pi_R = \delta\varphi_I = \delta\chi_I = 0$, this reduces to:

$$
\begin{aligned}
\rho_E =\ & (\rho_E)_0 + Q(r)\varphi_0\delta\varphi_R + (\Pi_I)_0\delta\Pi_I + \frac{\varphi_0'\delta\chi_R}{A_0\psi_0^4} \\
& + \frac{1}{2}\left[\delta\Pi_I^2 + \frac{\delta\chi_R^2}{A_0\psi_0^4} + Q(r)\delta\varphi_R^2\right] .
\end{aligned}
\tag{39}
$$

Notice now that, for any perturbation that falls into the star from outside, the energy density, and hence the total mass, will necessarily increase, as the linear terms in the expression above all vanish and we will be left with a positive definite contribution from the quadratic terms.

However, for internal perturbations we can again use the condition $\delta\Pi_I = -(\omega/\alpha_0)\,\delta\varphi_R$ introduced above to find:

$$
\begin{aligned}
\rho_E =\ & (\rho_E)_0 + \varphi_0\left(Q(r) - \frac{\omega^2}{\alpha_0^2}\right)\delta\varphi_R + \frac{\varphi_0'\delta\chi_R}{A_0\psi_0^4} \\
& + \frac{1}{2}\left[\left(Q(r) + \frac{\omega^2}{\alpha_0^2}\right)\delta\varphi_R^2 + \frac{\delta\chi_R^2}{A_0\psi_0^4}\right] ,
\end{aligned}
\tag{40}
$$

where we also already substituted $(\Pi_I)_0 = \omega\varphi_0/\alpha_0$. For small perturbations the linear contribution dominates, and it does not have a definite sign, so the total mass of the spacetime can increase or decrease.

In summary, we will consider three different types of perturbations for the simulations presented below, all of which will be such that $\delta\Pi_R = \delta\varphi_I = \delta\chi_I = 0$ (so that the initial momentum density vanishes).

- TYPE I: An *internal* perturbation such that $\delta\varphi_R \neq 0$ and $\delta\Pi_I = 0$. This perturbation changes the boson density.

- TYPE II: An *internal* perturbation such that $\delta\Pi_I = -(\omega/\alpha_0)\,\delta\varphi_R$. This perturbation preserves the boson density to linear order in small quantities, and can either increase or decrease the total mass of the star. Interestingly, in practice we have found that these type of perturbations also seem to have a very small effect on the value of the total mass.

- TYPE III: An *external* perturbation (scalar field falling into the star from outside) with $\delta\Pi_I = \pm(\omega/\alpha_0)\,\delta\varphi_R$, which again preserves the boson density to linear order in small quantities but always increases the mass.

Notice that in all three cases we have $\delta\varphi_R$ as a free parameter.

Finally, in order to find the perturbed initial data we choose values of ℓ and φ_0, and solve for the unperturbed configuration first. Having found the functions $\varphi(r)$, $A(r)$ and $\alpha(r)$ and the frequency ω for the unperturbed case, we add small perturbations to $\varphi(r)$ and $\Pi_I(r)$ corresponding to one of the three types described above (remember that for the unperturbed case we have $(\Pi_I)_0 = \omega\varphi_0/\alpha_0$), and solve again the Hamiltonian constraint to find the modified value of $A(r)$. We also solve again the polar slicing condition for a new lapse $\alpha(r)$, which will differ slightly from its unperturbed value $\alpha_0(r)$. This guarantees that the perturbed configuration will still be such that $\partial_t K_{\theta\theta} = 0$ initially (but this will not remain so at later times, as perturbed configurations are no longer stationary).

V. ANALYSIS TOOLS AND NUMERICAL CODE

A. Gauge choice

For our simulations we choose for simplicity a vanishing shift, and for the lapse function we choose the standard "1+log" slicing condition, which has the form [28]:

$$
\partial_t \alpha = -2\alpha K ,
\tag{41}
$$

where α is the lapse function and $K = K_m^m$ the trace of the extrinsic curvature. This condition is very robust in practice and allows for long-lived and stable evolutions.

Notice that the initial data, both in the perturbed and unperturbed case, is such that $K(t=0) = 0$ (in fact the whole extrinsic curvature vanishes). In the unperturbed case the 1+log slicing condition should guarantee that the lapse remains static up to numerical truncation error. For the perturbed cases, however, we expect K to evolve away from 0 from the beginning, resulting also in a dynamical lapse.

B. Total mass, boson number and binding energy

As already mentioned, the Eulerian observers measure an energy and boson density given by equations (19) and (20) above. These quantities can be used to define a total mass and conserved boson (particle) number.

For the total mass we go back to the Hamiltonian constraint, which in general has the form:

$$
R + K^2 - K_{ij}K^{ij} = 16\pi\rho_E ,
\tag{42}
$$

with R the three-dimensional Ricci scalar. Now, in spherical symmetry, and using the areal radius r_a^2, the spatial metric can be written as:

$$dl^2 = \frac{dr_a^2}{1 - 2m(r_a)/r_a} + r_a^2 d\Omega^2 , \qquad (43)$$

with $m(r_a)$ the so-called "Misner-Sharp mass function" [29]. In these coordinates the Ricci scalar becomes:

$$R = \left(\frac{4}{r_a^2}\right) \frac{dm}{dr_a} , \qquad (44)$$

so the Hamiltonian constraint implies:

$$\frac{dm}{dr_a} = r_a^2 \left[4\pi\rho_E + \frac{1}{4}\left(K_{ij}K^{ij} - K^2\right) \right] . \qquad (45)$$

The mass function can then be integrated to define a total mass M as:

$$M := \int_0^\infty \left[4\pi\rho_E + \frac{1}{4}\left(K_{ij}K^{ij} - K^2\right) \right] r_a^2 dr_a , \qquad (46)$$

where $K_{ij}K^{ij} = (K_r^r)^2 + 2(K_\theta^\theta)^2$. Notice that if $K_{ij} = 0$ the above expression is essentially identical to the Newtonian definition of mass (but we need to be in the areal gauge). Now, if the sources have compact support (or decay exponentially), the spacetime will reduce to Schwarzschild far away, and M will correspond to the total ADM mass of the system.

On the other hand, the areal radius is given in terms of our coordinate radius r as $r_a = r\psi^2 B^{1/2}$ (confront (43) with (2)), which implies:

$$r_a^2 dr_a = r^2\psi^6 B^{3/2}\left[1 + r\left(\frac{\partial_r B}{2B} + 2\frac{\partial_r \psi}{\psi}\right)\right] dr . \qquad (47)$$

The final expression for the total mass is then:

$$\begin{aligned} M := & \int_0^\infty r^2\psi^6 B^{3/2}\left[4\pi\rho_E + \frac{1}{4}\left(K_{ij}K^{ij} - K^2\right)\right] \\ & \times \left[1 + r\left(\frac{\partial_r B}{2B} + 2\frac{\partial_r \psi}{\psi}\right)\right] dr , \end{aligned} \qquad (48)$$

This expression is valid for any spherically symmetric metric parametrized as in Eq. (2).

Let us turn now to the total boson number. For a complex scalar field it is well known that there exists a conserved current particle J^μ such that $\nabla_\mu J^\mu = 0$ (see Eq. (21) above). This immediately implies that the integral of the boson density $\rho_B = -n^\mu J_\mu$ is a conserved quantity, which we refer to as the "total boson number" N_B:

$$\begin{aligned} N_B := & \int \rho_B \gamma^{1/2} dr d\theta d\varphi \\ = & 4\pi \int_0^\infty \rho_B \left(A^{1/2}B\psi^6\right) r^2 dr , \end{aligned} \qquad (49)$$

with $\gamma = AB^2\psi^{12}$ the determinant of the spatial metric. Notice that if the boson particles associated with the complex scalar fields had an electric charge q, the total charge would simply be $Q = qN_B$.

One last concept that needs to be introduced is that of "binding energy". The binding energy U is a measure of the difference between the total mass-energy of the system, given by the ADM mass M, and the rest mass of the bosons, which can be simply defined as μN_B, with μ the mass of the scalar field:

$$U := M - \mu N_B . \qquad (50)$$

If the binding energy is negative, we should have a bound gravitational system, while if it is positive the system is unbound.

C. Apparent horizons and horizon mass

As we will see below, when we perturb boson stars in the unstable branch they can collapse to form a black hole. We identify the presence of such a black hole by looking for the appearance of an apparent horizon, that is the outermost closed two-surface where the expansion of outgoing null geodesics vanishes. In the case of spherical symmetry this is rather straightforward, and reduces to the following condition [28]:

$$\frac{1}{\psi^2\sqrt{A}}\left(\frac{2}{r} + \frac{\partial_r B}{B} + 4\frac{\partial\psi}{\psi}\right) - 2K_\theta^\theta = 0 . \qquad (51)$$

Notice that the above equation should not be understood as a differential equation, but rather as an algebraic condition that, when satisfied for some value of r, indicates the presence of an apparent horizon at that location. If the condition is satisfied at more than one place, the apparent horizon will correspond to the outermost location.

Once we have located an apparent horizon at some coordinate radius $r = r_H$ we can calculate its area as $A_H = 4\pi r_a^2 = 4\pi r_H^2 \psi_H^4 B_H$, with r_a the areal radius as before, and from there obtain the so-called "horizon mass" as follows:

$$M_H = \sqrt{\frac{A_H}{16\pi}} = \frac{r_H\psi_H^2 B_H^{1/2}}{2} . \qquad (52)$$

This horizon mass should always be smaller than, or equal to, the total ADM mass M of the spacetime.

D. Numerical code

Our simulations are carried out with the *OllinSphere* code, a generic numerical relativity finite-difference code for spherical symmetry. The initial data is obtained using a shooting method with fourth order Runge-Kutta on a

regular grid. Our grid staggers the origin to avoid having divisions by zero for terms of type $1/r$.

For the evolution we use a BSSN formulation adapted to spherical symmetry [27]. The code uses a method of lines with fourth order spatial differences, and a fourth order Runge-Kutta time integrator. This code has been previously tested with real scalar fields, and has been used in the context of scalar-tensor theories of gravity with minimal modifications [30, 31]. The exterior boundary conditions are of a constraint-preserving type, following the method described in [32].

VI. NUMERICAL SIMULATIONS

A. General considerations

We have performed a series of dynamical simulations for ℓ-boson stars, for different value of ℓ in the range $\ell = 0, 1, 2, 3, 4$. In each case we have performed simulations of both the unperturbed solutions, and different perturbations of the three types discussed above in Section IV. In all cases considered here we have chosen for simplicity the boson mass equal to unity, $\mu = 1$.

Before going into our results, there are several properties of the ℓ-boson stars that need to be discussed. As mentioned above, for a fixed value of ℓ the scalar field close to the origin behaves as $\varphi(r) \sim \varphi_0 r^\ell$, and for each value of φ_0 one needs to solve an eigenvalue problem to find the oscillation frequency ω. Parametrizing the solutions for each ℓ with φ_0, one finds that as we increase φ_0 the ADM mass M of the configurations first increases and reaches a maximum, after which it decreases again. These results where already presented in [20].

In that reference, however, we did not compute the total boson number N_B and binding energy U for each solution. Doing that we find that the boson number increases with φ_0 until it reaches a maximum at the same point as the total mass M, and then also decreases. The binding energy U, on the other hand, starts negative and decreases, until it reaches a minimum just as the mass and boson number reach a maximum. It then starts to increase and at some point becomes positive, corresponding to solutions that are no longer gravitationally bound.

Figure 1 shows a plot of the total ADM mass M, total boson number N_B, and binding energy U for the case with $\ell = 1$. The configurations here are parametrized with a_0, which is given in terms of φ_0 as $a_0 = [4\pi(2\ell + 1)]^{1/2}\varphi_0$ (this is in order to be consistent with the normalization used in [20]). Notice how there is a region where $M < N_B$ corresponding to bound configurations, and a region with $M > N_B$ corresponding to unbound states. Similar plots can be found for other values of ℓ.

For each value of ℓ, there are then three regions of interest in the parameter space of solutions: stable bound configurations with $M < M_{\max}$ and $M < N_B$, unstable bound configurations with $M > M_{\max}$ and $M < N_B$, and
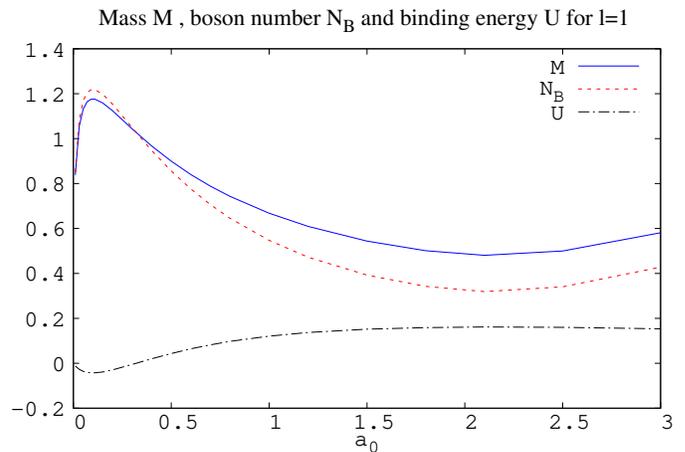

FIG. 1: Total ADM mass M, total boson number N_B, and binding energy U for the case for $\ell = 1$ and $\mu = 1$. The configurations here are parametrized with a_0, which is given in terms of φ_0 as $a_0 = [4\pi(2\ell + 1)]^{1/2}\varphi_0$.

finally unstable unbound configurations with $M > M_{\max}$ and $M > N_B$.

B. Summary of results

As mentioned above, for each value of ℓ there are three regions of interest in parameter space: stable configurations, unstable bound configurations, and unstable unbound configurations. Let us denote by φ_0^M the value of the parameter φ_0 for which we obtain the maximum ADM mass, and by φ_0^U the value for which the binding energy is zero. We find that in general $\varphi_0^M < \varphi_0^U$.

For all values of ℓ we have studied, the results of our simulations can be summarized as follows:

- The region $0 < \varphi_0 < \varphi_0^M$ corresponds to bound stable configurations. For all types of (small) perturbations studied, these configurations oscillate around the stationary solution. The oscillations are extremely long-lived, but they seem to slowly settle down to a stationary solution that lies close to the original one.

- The region $\varphi_0^M < \varphi_0 < \varphi_0^U$ corresponds to unstable but bound configurations that, depending on the specific type of perturbation, can either collapse to form a black hole or "migrate" to the stable branch. This migration to the stable branch is achieved by ejecting excess scalar field to infinity. Again, these migrating solutions in fact oscillate for extremely long times and seem to very slowly settle down to a stationary solution.

- The region $\varphi_0 > \varphi_0^U$ corresponds to unstable and unbound solutions that, depending on the specific type of perturbation, can either collapse to a black
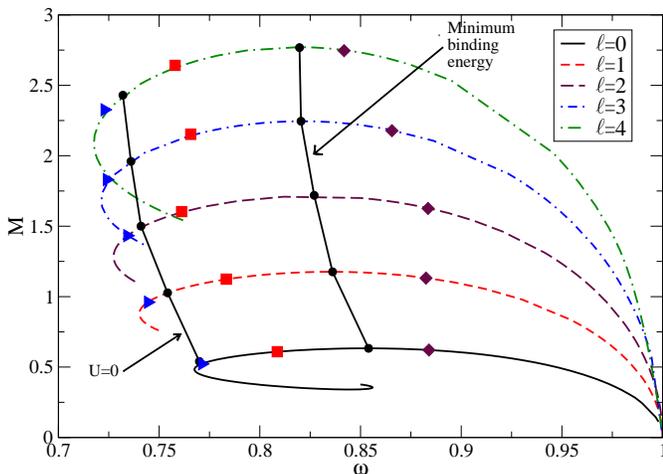
FIG. 2: The three regions of stability for ℓ-boson stars. See the text for a detailed explanation.

hole or dissipate ("explode") to infinity. Dissipating solutions may oscillate a few times before they dissipate completely.

For standard boson stars with $\ell = 0$, the difference in behaviour between bound and unbound unstable configurations that do not collapse to form a black hole, that is configurations that either migrate to the stable branch or dissipate to infinity, has already been observed [33–35]. Interestingly, in one of the original papers on perturbed $\ell = 0$ boson stars by Seidel and Suen [36], the authors mention that they observe no difference between unstable configurations with negative or positive binding energy. This could be related to the specific types of perturbations they studied.

Tables I to V present results from a battery of simulations we have performed for values of ℓ in the range $\ell = 0, 1, 2, 3, 4$. In each case, we have considered all three types of perturbations described in Section IV above. We have added also perturbations of "type 0", which in fact correspond to evolutions of the unperturbed initial data. Notice that these "unperturbed" evolutions are in fact slightly perturbed by numerical truncation error.

Figure 2 shows the three regions of stability for $\ell = 0, 1, 2, 3, 4$. The figure shows a plot of the mass of the configuration M as a function of the oscillation frequency ω. Configurations to the right of the maximum mass line (which coincides with the minimum binding energy) correspond to bound stable configurations. The diamonds indicate those specific stable configurations that where evolved. The central region corresponds to unstable but bound configurations. Squares represent those specific configurations that were evolved in this region, and either collapse to a black hole or migrate to a stable configuration. Finally, all those configurations to the left of the $U = 0$ line (zero binding energy) correspond to unstable and unbound solutions. The triangles correspond to those specific configurations that we evolved,

and either collapse to a black hole or disperse to infinity.

In all our simulations, we used a small Gaussian perturbation to the scalar field $\delta\varphi_R$:

$$\delta\varphi_R(r) = \epsilon \, \exp\left[-(r - r_0)/\sigma^2\right] \,, \qquad (53)$$

with ϵ the amplitude of the perturbation and σ its width. When the perturbations are internal to the star (types I and II), we choose r_0 to coincide roughly with the place where the scalar field $\varphi(r)$ has a maximum (notice that for $\ell > 0$ this maximum is not at the origin). The amplitude of the perturbation is rescaled with this maximum, and for simplicity we always take the width of the Gaussian to be equal to unity, $\sigma = 1$. For the perturbation of the imaginary part of the time derivative of the scalar field, $\Pi_I(r)$, we take

$$\delta\Pi_I(r) = s \, (\omega/\alpha) \, \delta\varphi_R(r), \qquad (54)$$

with $s = 0$ for perturbations of type I, $s = -1$ for type II, and $s = \pm 1$ for type III.

In all the simulations described here we have taken a grid spacing of $\Delta r = 0.02$ and a total of 2500 grid points, so the outer boundary is located at $r = 49.99$ (remember that we stagger the origin). For the time stepping we take $\Delta t = 0.01$, and we evolve for $50,000$ time steps, corresponding to a final time $t = 500$. We have in fact performed simulations with different grid spacings to verify fourth order convergence, and also much longer simulations in some special cases to study the late time behaviour of solutions that migrate to the stable branch or explode to infinity (see Section VI C below). The main effect of using a higher resolution is that those perturbations of type 0 that collapse to a black hole do so at later times for higher resolution runs. This is to be expected since in that case the perturbation is only through numerical truncation error which is smaller for higher resolution.

From the tables one can see some interesting facts. First, for all types of (small) perturbations with $0 < \varphi_0 < \varphi_0^M$, and all values of ℓ, the configurations are stable as expected. In the region $\varphi_0^M < \varphi_0 < \varphi_0^U$, the configurations are unstable and either collapse to a black hole or migrate to the stable branch. But collapse to a black hole is far more common, and we find that only type I perturbations with $\epsilon < 0$, or type II perturbations with $\epsilon > 0$ can migrate to the stable branch. Moreover, for type II perturbations with $\epsilon > 0$, migration to the stable branch only happens for very small values of ϵ, and increasing slightly the perturbation amplitude again results in collapse to a black hole. The transition between migration and collapse for these type of perturbations seems to be related not so much with the sign of the binding energy U, which in these region is always negative, but rather with the value of $dU/d\epsilon$ (that is, if U is decreasing or increasing with ϵ), but this still needs more studying. Finally, in the region $\varphi_0 > \varphi_0^U$ the configurations are also unstable and either collapse to a black hole of explode to infinity. Again, collapse is far more common and only

type I perturbations with $\epsilon < 0$, or type II perturbations with $\epsilon > 0$ (and very small) explode to infinity.

Interestingly, for type 0 perturbations in the unstable branch $\varphi_0 > \varphi_0^M$, we always find collapse to a black hole except for one particular case with $\ell = 3$ for which the configuration migrates to the stable branch. Of course, these perturbations are only through numerical truncation error which we can not control.

C. Examples of our simulations

In the Section we present some representative examples of our numerical simulations. All the simulations shown here correspond to the case of $\ell = 2$. For other values of ℓ the results are qualitatively similar.

We will show the results of four particular simulations, corresponding to those configurations marked as (A, B, C, D) in table III. Figure 3 shows the initial value of $\varphi_R(r)$ for these four configurations. Configuration A corresponds to a perturbation of a stable solution, configuration B to a perturbation of an unstable but bound solution, while configurations C and D correspond to different perturbations of the same unstable and unbound solution. Notice that configurations C and D are almost identical since they are different perturbations of the same stationary solution. Configuration C adds a small Gaussian close to the peak, while configuration D adds one outside the star at $r = 30$ (this is barely visible in the plot). Figure 4 shows the initial position of these four configurations on the $\ell = 2$ mass-frequency diagram (compare with figure 2 for $\ell = 2$). In the figure we also show the position of the maximum mass (minimum binding energy), and the place where the binding energy U changes sign. Also shown is the approximate final state of configuration B after it migrates to the stable branch (see below).

Let us now focus on configuration A, which corresponds to a perturbation of type II of a solution in the stable branch, with a positive perturbation amplitude of 1% at the peak of the scalar field. This configuration was run for $50,000$ times steps of size $\Delta t = 0.01$, resulting in a final time $T = 500$. Some results for this simulation are shown in figure 5. The top-left panel of the figure shows the minimum value of the lapse. We can see that after an initial perturbation, it settles back down to a value very close to the original one, and has very small oscillations for the rest of the run. The top-right panel shows the value of the maximum value of the norm of the scalar field $|\varphi| := \sqrt{\varphi\varphi^*}$. Again we see that there are small oscillations around its initial value. Notice that for the stationary solution the norm is in fact independent of time even if the scalar field is oscillating. The bottom-left panel shows the value of the total integrated mass M at the boundary. Notice that initially it remains constant until $t \sim 50$. This is to be expected since for this run the boundary is located precisely at $r = 50$, and the scalar perturbation takes this long to reach it.
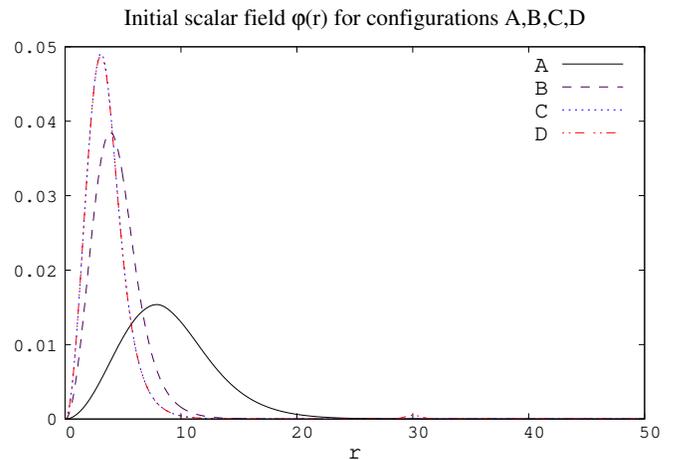
FIG. 3: Initial value of the real part of the scalar field $\varphi_R(r)$ for the configurations (A, B, C, D) of table III. Notice that configurations C and D are almost identical, since they represent small (but different) perturbations of the same stationary solution.
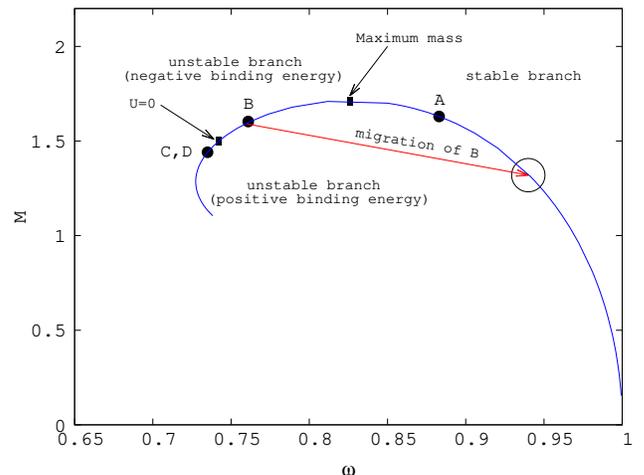
FIG. 4: Initial positions on the $\ell = 2$ mass-frequency diagram for the configurations (A, B, C, D) of table III. The black dots correspond to the initial (unperturbed) states, and the black squares mark the position of the maximum mass (minimum binding energy), and the place where the binding energy U changes sign. Notice again that configurations C and D start from the same location, as they are different perturbations of the same stationary solution. Also shown is the approximate final state of configuration B after it migrates to the stable branch (see text for details).

After this time, the mass decreases slightly and then settles down to a smaller value. This indicates that a small pulse of scalar field has been ejected by the star to infinity. Finally, the bottom-right panel shows the total integrated boson number N_B at the boundary. Again, we see that it remains constant until the ejected pulse reaches the boundary at $t \sim 50$, it then increases slightly and settles down to a higher value. This shows that the

ℓ	a_0	ω	Perturbation	M	N_B	U	$\epsilon/\varphi_R^{\max}$	s	r_0	End result
0	0.2	0.88401	Type 0	0.6209	0.6391	-0.0182	$-$	$-$	$-$	stable
0	0.2	0.88401	Type I	0.6211	0.6394	-0.0183	$+0.005$	0	0.0	stable
0	0.2	0.88401	Type I	0.6207	0.6389	-0.0182	-0.005	0	0.0	stable
0	0.2	0.88401	Type II	0.6209	0.6391	-0.0182	$+0.005$	-1	0.0	stable
0	0.2	0.88401	Type II	0.6209	0.6391	-0.0182	-0.005	-1	0.0	stable
0	0.2	0.88401	Type III	0.6238	0.6412	-0.0174	$+0.01$	$+1$	20.0	stable
0	0.2	0.88401	Type III	0.6237	0.6372	-0.0135	$+0.01$	-1	20.0	stable
0	0.4	0.80866	Type 0	0.6088	0.6235	-0.0147	$-$	$-$	$-$	black hole
0	0.4	0.80866	Type I	0.6096	0.6246	-0.0150	$+0.005$	0	0.0	black hole
0	0.4	0.80866	Type I	0.6079	0.6225	-0.0146	-0.005	0	0.0	migration to stable branch
0	0.4	0.80866	Type II	0.6087	0.6235	-0.0148	$+0.005$	-1	0.0	migration to stable branch
0	0.4	0.80866	Type II	0.6088	0.6236	-0.0148	-0.005	-1	0.0	black hole
0	0.4	0.80866	Type III	0.6193	0.6305	-0.0112	$+0.01$	$+1$	20.0	black hole
0	0.4	0.80866	Type III	0.6193	0.6166	$+0.0027$	$+0.01$	-1	20.0	black hole
0	0.6	0.77134	Type 0	0.5248	0.5167	$+0.0081$	$-$	$-$	$-$	black hole
0	0.6	0.77134	Type I	0.5266	0.5190	$+0.0075$	$+0.005$	0	0.0	black hole
0	0.6	0.77134	Type I	0.5230	0.5144	$+0.0086$	-0.005	0	0.0	explosion to infinity
0	0.6	0.77134	Type II	0.5246	0.5165	$+0.0081$	$+0.005$	-1	0.0	explosion to infinity
0	0.6	0.77134	Type II	0.5250	0.5169	$+0.0081$	-0.005	-1	0.0	black hole
0	0.6	0.77134	Type III	0.5481	0.5314	$+0.0167$	$+0.01$	$+1$	20.0	black hole
0	0.6	0.77134	Type III	0.5480	0.5020	$+0.0460$	$+0.01$	-1	20.0	black hole

TABLE I: Results of simulations for $\ell = 0$. Notice that in this case the maximum mass is $M_{\max} \simeq 0.633$.

ℓ	a_0	ω	Perturbation	M	N_B	U	$\epsilon/\varphi_R^{\max}$	s	r_0	End result
1	0.05	0.88253	Type 0	1.1316	1.1674	-0.0358	$-$	$-$	$-$	stable
1	0.05	0.88253	Type I	1.1344	1.1705	-0.0361	$+0.01$	0	4.5	stable
1	0.05	0.88253	Type I	1.1288	1.1642	-0.0354	-0.01	0	4.5	stable
1	0.05	0.88253	Type II	1.1316	1.1673	-0.0357	$+0.01$	-1	4.5	stable
1	0.05	0.88253	Type II	1.1316	1.1673	-0.0357	-0.01	-1	4.5	stable
1	0.05	0.88253	Type III	1.1324	1.1681	-0.0357	$+0.01$	$+1$	20.0	stable
1	0.05	0.88253	Type III	1.1320	1.1670	-0.0350	$+0.01$	-1	20.0	stable
1	0.2	0.78330	Type 0	1.1241	1.1536	-0.0295	$-$	$-$	$-$	black hole
1	0.2	0.78330	Type I	1.1297	1.1608	-0.0311	$+0.01$	0	2.5	black hole
1	0.2	0.78330	Type I	1.1185	1.1465	-0.0280	-0.01	0	2.5	migration to stable branch
1	0.2	0.78330	Type II	1.1240	1.1536	-0.0296	$+0.005$	-1	2.5	migration to stable branch
1	0.2	0.78330	Type II	1.1241	1.1535	-0.0294	$+0.01$	-1	2.5	black hole
1	0.2	0.78330	Type II	1.1242	1.1537	-0.0295	-0.01	-1	2.5	black hole
1	0.2	0.78330	Type III	1.1261	1.1550	-0.0289	$+0.01$	$+1$	20.0	black hole
1	0.2	0.78330	Type III	1.1261	1.1522	-0.0261	$+0.01$	-1	20.0	black hole
1	0.4	0.74471	Type 0	0.9674	0.9476	$+0.0198$	$-$	$-$	$-$	black hole
1	0.4	0.74471	Type I	0.9743	0.9568	$+0.0175$	$+0.01$	0	1.7	black hole
1	0.4	0.74471	Type I	0.9606	0.9385	$+0.0221$	-0.01	0	1.7	explosion to infinity
1	0.4	0.74471	Type II	0.9673	0.9473	$+0.0200$	$+0.01$	-1	1.7	explosion to infinity
1	0.4	0.74471	Type II	0.9677	0.9478	$+0.0199$	-0.01	-1	1.7	black hole
1	0.4	0.74471	Type III	0.9714	0.9502	$+0.0212$	$+0.01$	$+1$	20.0	black hole
1	0.4	0.74471	Type III	0.9714	0.9450	$+0.0264$	$+0.01$	-1	20.0	black hole

TABLE II: Results of simulations for $\ell = 1$. Notice that in this case the maximum mass is $M_{\max} \simeq 1.176$.

ℓ	a_0	ω	Perturbation	M	N_B	U	$\epsilon/\varphi_R^{\max}$	s	r_0	End result
2	0.005	0.88354	Type 0	1.6268	1.6793	−0.0525	−	−	−	stable
2	0.005	0.88354	Type I	1.6307	1.6837	−0.0530	+0.01	0	8.0	stable
2	0.005	0.88354	Type I	1.6229	1.6749	−0.0520	−0.01	0	8.0	stable
2	0.005	0.88354	(A) Type II	1.6268	1.6792	−0.0524	+0.01	−1	8.0	stable
2	0.005	0.88354	Type II	1.6268	1.6793	−0.0525	−0.01	−1	8.0	stable
2	0.005	0.88354	Type III	1.6273	1.6797	−0.0524	+0.01	+1	30.0	stable
2	0.005	0.88354	Type III	1.6273	1.6789	−0.0516	+0.01	−1	30.0	stable
2	0.05	0.76114	Type 0	1.6035	1.6388	−0.0353	−	−	−	black hole
2	0.05	0.76114	Type I	1.6121	1.6502	−0.0381	+0.01	0	4.0	black hole
2	0.05	0.76114	(B) Type I	1.5949	1.6276	−0.0327	−0.01	0	4.0	migration to stable branch
2	0.05	0.76114	Type II	1.6035	1.6388	−0.0353	+0.005	−1	4.0	migration to stable branch
2	0.05	0.76114	Type II	1.6035	1.6387	−0.0352	+0.01	−1	4.0	black hole
2	0.05	0.76114	Type II	1.6036	1.6389	−0.0353	−0.01	−1	4.0	black hole
2	0.05	0.76114	Type III	1.6062	1.6407	−0.0345	+0.01	+1	30.0	black hole
2	0.05	0.76114	Type III	1.6062	1.6370	−0.0308	+0.01	−1	30.0	black hole
2	0.1	0.73427	Type 0	1.4424	1.4231	+0.0193	−	−	−	black hole
2	0.1	0.73427	Type I	1.4521	1.4363	+0.0158	+0.01	0	3.0	black hole
2	0.1	0.73427	Type I	1.4328	1.4100	+0.0228	−0.01	0	3.0	explosion to infinity
2	0.1	0.73427	(C) Type II	1.4424	1.4230	+0.0194	+0.005	−1	3.0	explosion to infinity
2	0.1	0.73427	Type II	1.4424	1.4229	+0.0195	+0.01	−1	3.0	black hole
2	0.1	0.73427	Type II	1.4426	1.4232	+0.0194	−0.01	−1	3.0	black hole
2	0.1	0.73427	(D) Type III	1.4466	1.4258	+0.0208	+0.01	+1	30.0	black hole
2	0.1	0.73427	Type III	1.4466	1.4203	+0.0263	+0.01	−1	30.0	black hole

TABLE III: Results of simulations for $\ell = 2$. Notice that in this case the maximum mass is $M_{\max} \simeq 1.714$.

ℓ	a_0	ω	Perturbation	M	N_B	U	$\epsilon/\varphi_R^{\max}$	s	r_0	End result
3	0.0005	0.86561	Type 0	2.1782	2.2560	−0.0778	−	−	−	stable
3	0.0005	0.86561	Type I	2.1835	2.2621	−0.0786	+0.01	0	10.0	stable
3	0.0005	0.86561	Type I	2.1729	2.2500	−0.0771	−0.01	0	10.0	stable
3	0.0005	0.86561	Type II	2.1782	2.2560	−0.0778	+0.01	−1	10.0	stable
3	0.0005	0.86561	Type II	2.1782	2.2560	−0.0778	−0.01	−1	10.0	stable
3	0.0005	0.86561	Type III	2.1787	2.2564	−0.0777	+0.01	+1	30.0	stable
3	0.0005	0.86561	Type III	2.1786	2.2558	−0.0772	+0.01	−1	30.0	stable
3	0.005	0.76579	Type 0	2.1519	2.2159	−0.0640	−	−	−	migration to stable branch
3	0.005	0.76579	Type I	2.1621	2.2291	−0.0670	+0.01	0	6.0	black hole
3	0.005	0.76579	Type I	2.1419	2.2028	−0.0609	−0.01	0	6.0	migration to stable branch
3	0.005	0.76579	Type II	2.1519	2.2159	−0.0640	+0.002	−1	6.0	migration to stable branch
3	0.005	0.76579	Type II	2.1520	2.2158	−0.0638	+0.01	−1	6.0	black hole
3	0.005	0.76579	Type II	2.1521	2.2159	−0.0638	−0.01	−1	6.0	black hole
3	0.005	0.76579	Type III	2.1534	2.2170	−0.0636	+0.01	+1	30.0	black hole
3	0.005	0.76579	Type III	2.1534	2.2149	−0.0615	+0.01	−1	30.0	black hole
3	0.02	0.72405	Type 0	1.8432	1.7997	+0.0435	−	−	−	black hole
3	0.02	0.72405	Type I	1.8558	1.8170	+0.0388	+0.01	0	4.0	black hole
3	0.02	0.72405	Type I	1.8308	1.7826	+0.0482	−0.01	0	4.0	explosion to infinity
3	0.02	0.72405	Type II	1.8432	1.7997	+0.0435	+0.005	−1	4.0	explosion to infinity
3	0.02	0.72405	Type II	1.8432	1.7995	+0.0437	+0.01	−1		black hole
3	0.02	0.72405	Type II	1.8435	1.7998	+0.0437	−0.01	−1		black hole
3	0.02	0.72405	Type III	1.8462	1.8017	+0.0445	+0.01	+1	30.0	black hole
3	0.02	0.72405	Type III	1.8462	1.7978	+0.0484	+0.01	−1	30.0	black hole

TABLE IV: Results of simulations for $\ell = 3$. Notice that in this case the maximum mass is $M_{\max} \simeq 2.245$.

ℓ	a_0	ω	Perturbation	M	N_B	U	$\epsilon/\varphi_R^{\max}$	s	r_0	End result
4	0.00005	0.84185	Type 0	2.7458	2.8536	−0.1078	−	−	−	stable
4	0.00005	0.84185	Type I	2.7531	2.8622	−0.1091	+0.01	0	11.5	stable
4	0.00005	0.84185	Type I	2.7385	2.8449	−0.1064	−0.01	0	11.5	stable
4	0.00005	0.84185	Type II	2.7459	2.8535	−0.1076	+0.01	−1	11.5	stable
4	0.00005	0.84185	Type II	2.7459	2.8535	−0.1076	−0.01	−1	11.5	stable
4	0.00005	0.84185	Type III	2.7463	2.8540	−0.1077	+0.01	+1	30.0	stable
4	0.00005	0.84185	Type III	2.7462	2.8533	−0.1071	+0.01	−1	30.0	stable
4	0.0005	0.75793	Type 0	2.6419	2.7181	−0.0762	−	−	−	black hole
4	0.0005	0.75793	Type I	2.6539	2.7339	−0.0800	+0.01	0	7.5	black hole
4	0.0005	0.75793	Type I	2.6299	2.7024	−0.0725	−0.01	0	7.5	migration to stable branch
4	0.0005	0.75793	Type II	2.6419	2.7181	−0.0762	+0.005	−1	7.5	migration to stable branch
4	0.0005	0.75793	Type II	2.6419	2.7180	−0.0761	+0.01	−1	7.5	black hole
4	0.0005	0.75793	Type II	2.6420	2.7181	−0.0761	−0.01	−1	7.5	black hole
4	0.0005	0.75793	Type III	2.6430	2.7190	−0.0760	+0.01	+1	30.0	black hole
4	0.0005	0.75793	Type III	2.6430	2.7173	−0.0743	+0.01	−1	30.0	black hole
4	0.002	0.72290	Type 0	2.3411	2.3117	+0.0294	−	−	−	black hole
4	0.002	0.72290	Type I	2.3556	2.3318	+0.0238	+0.01	0	5.5	black hole
4	0.002	0.72290	Type I	2.3267	2.2918	+0.0349	−0.01	0	5.5	explosion to infinity
4	0.002	0.72290	Type II	2.3411	2.3116	+0.0295	+0.005	−1	5.5	explosion to infinity
4	0.002	0.72290	Type II	2.3411	2.3115	+0.0296	+0.01	−1	5.5	black hole
4	0.002	0.72290	Type II	2.3413	2.3118	+0.0295	−0.01	−1	5.5	black hole
4	0.002	0.72290	Type III	2.3430	2.3131	+0.0299	+0.01	+1	30.0	black hole
4	0.002	0.72290	Type III	2.3430	2.3104	+0.0326	+0.01	−1	30.0	black hole

TABLE V: Results of simulations for $\ell = 4$. Notice that in this case the maximum mass is $M_{\max} \simeq 2.771$.

ejected scalar field in fact has *negative* bosonic charge (in a quantum mechanical interpretation it would be made of anti-particles). The configuration is clearly stable, and after the initial perturbation settles down to a new configuration very close to the original one.

Consider next configuration B, which corresponds to a type I perturbation of an unstable but gravitationally bound solution. The perturbation again has an amplitude of 1% at the peak of the scalar field, but in this case it is *negative*, that is, it decreases slightly the size of the peak. This is an example of an unstable solution that migrates to the stable branch. For this reason we have in fact continued the simulation for a total of one million time steps, reaching a final time of $T = 10,000$. Results for this simulation are shown in figure 6, where the four panels show the same quantities as before. The figure shows that the evolution is now considerably more interesting. Notice first the minimum value of the lapse (top-left panel). It starts at a value of ~ 0.57, but rapidly increases and starts oscillating between 0.8 and 0.93. These oscillations have a very long period of about $\Delta T \sim 630$, corresponding to a frequency much smaller than that of oscillations of the scalar field. The oscillations also seem to be very slowly decreasing in amplitude, indicating that the evolution will eventually settle down to a stationary configuration after an extremely long time, though as mentioned before, at this point we can not rule out the

possibility that the configuration will instead settle to some type of multi-oscillating solution [11]. Something very similar happens to the maximum norm of the scalar field (top-right panel), which starts at a value of ~ 0.038, and rapidly drops and starts oscillating around ~ 0.01, with the same long period as the lapse. Here we can also see some very small oscillations superposed to the large ones, with a very short period, corresponding to the natural oscillations of the scalar field (see inset in top-right panel for a zoom of a small region of the plot). Again, the large oscillations appear to be slowly decaying in amplitude. When we look at the total integrated mass M and boson number N_B (bottom two panels), we notice that they are both decreasing in time, but they do so in steps that become smaller and smaller with time. They also seem to be slowly converging to smaller values. The steps indicate that the boson star is ejecting pulses of scalar field (with positive bosonic charge) one at a time, with a period that matches the oscillations of the lapse function. The configurations clearly seems to have migrated to the stable branch after ejecting excess scalar field in a series of pulses, and is very slowly settling down.

For this particular configuration we in fact have also performed a much longer simulation with 10 million time steps (reaching a final time of $T = 100,000$) in an attempt to determine the final state, but we have found
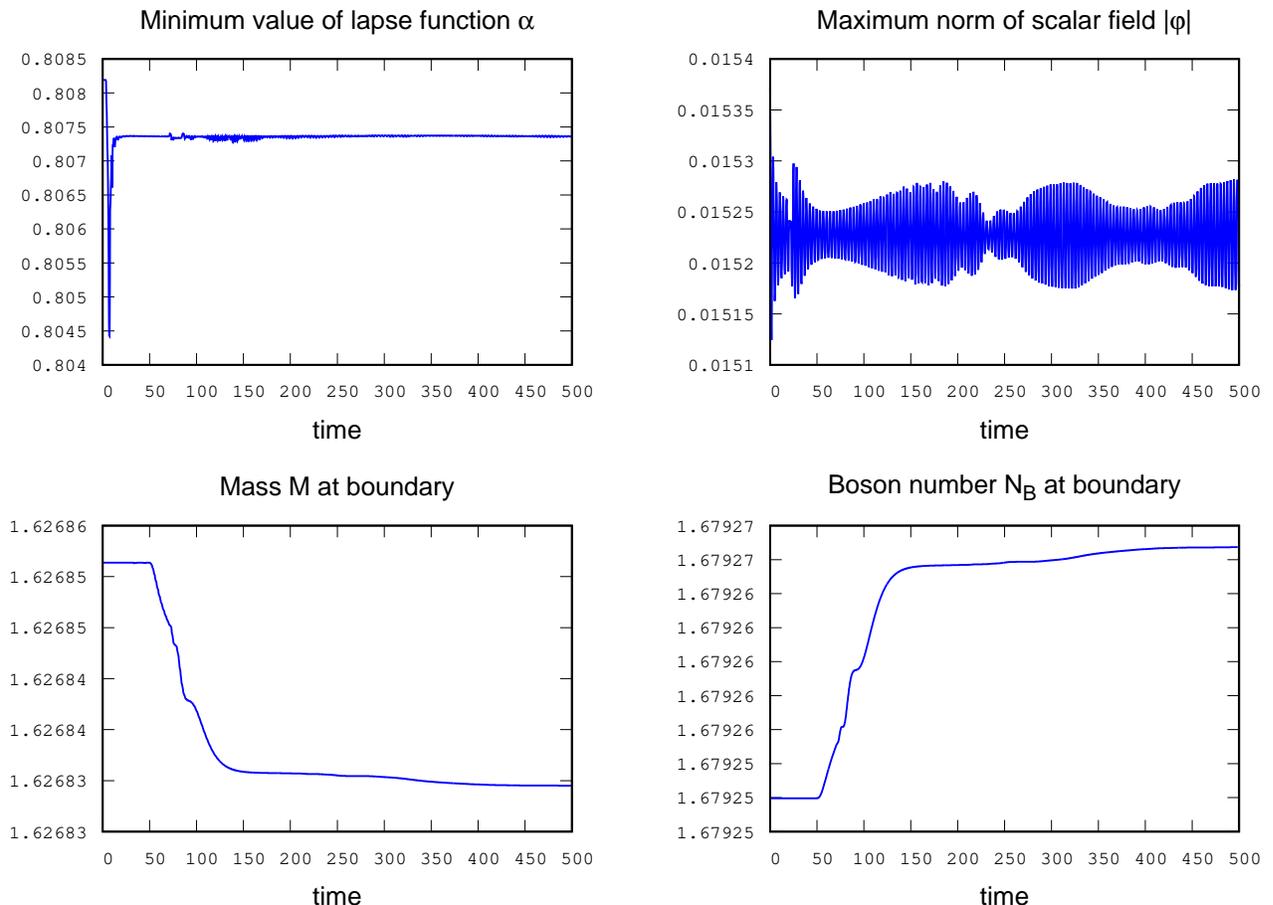
FIG. 5: Evolution in time of configuration A. This is a stable configuration. The different panels show: Minimum of the lapse function $\alpha_{\min}$ (top-left), maximum norm of the scalar field $|\varphi|_{\max}$ (top-right), integrated mass M at the outer boundary (bottom-left), and integrated boson number N_B at the outer boundary (bottom-right).

that at the end of this extremely long simulation the configuration has yet to settle completely down. Our best estimate for the final state is then only approximate. By the end of this simulation the total integrated mass is $M \sim 1.33$ and still slowly falling, while the central value of the lapse is oscillating between 0.87 and 0.92. Our best estimate of the final state can then be obtained by assuming a final central lapse of $\alpha(r = 0) \sim 0.9$, which corresponds to a stationary solution with frequency $\omega \sim 0.94$, ADM mass $M \sim 1.31$ and total boson number $N_B \sim 1.33$ (this final configuration is shown as the open circle in figure 4).

Let us now move to configuration C, which corresponds to a type II perturbation of an unstable and unbound solution. In this case the perturbation adds a Gaussian with a small amplitude equivalent to only 0.5% of the maximum value of the scalar field. This is an example of an unstable and unbound solution that explodes to infinity. Just as we did for configuration B, we have again continued the simulation for one million time steps, reaching a final time of $T = 10,000$. Results for this simulation are shown in figure 7. Notice that the evolution

is now very different from that of configuration B. The minimum of the lapse grows rapidly from an initial value of ~ 0.5, and after a few small oscillations becomes 1, indicating that the spacetime is essentially Minkowski. At the same time, the maximum norm of the scalar field drops from its initial value, and after a few oscillations goes to zero. The total mass and boson number measured at the boundary first remain constant until $T \sim 250$. They both then drop rapidly, and after a series of steps also reach zero. The scalar field corresponding to the boson star has then escaped completely to infinity, leaving behind empty Minkowski spacetime. The fact that the total mass and boson number at the boundary only begins to fall at $T \sim 250$ shows that there is a delay, and the boson star does not begin to dissipate immediately, as otherwise one would see effects at the boundary after one light-crossing time, that is $T \sim 50$ (remember that the boundary is located at $r = 50$).

Finally, consider configuration D. This corresponds to a type III perturbation of the *same* unstable and unbound solution of configuration C. We now perturb the star with a small Gaussian with an amplitude of 1% of the
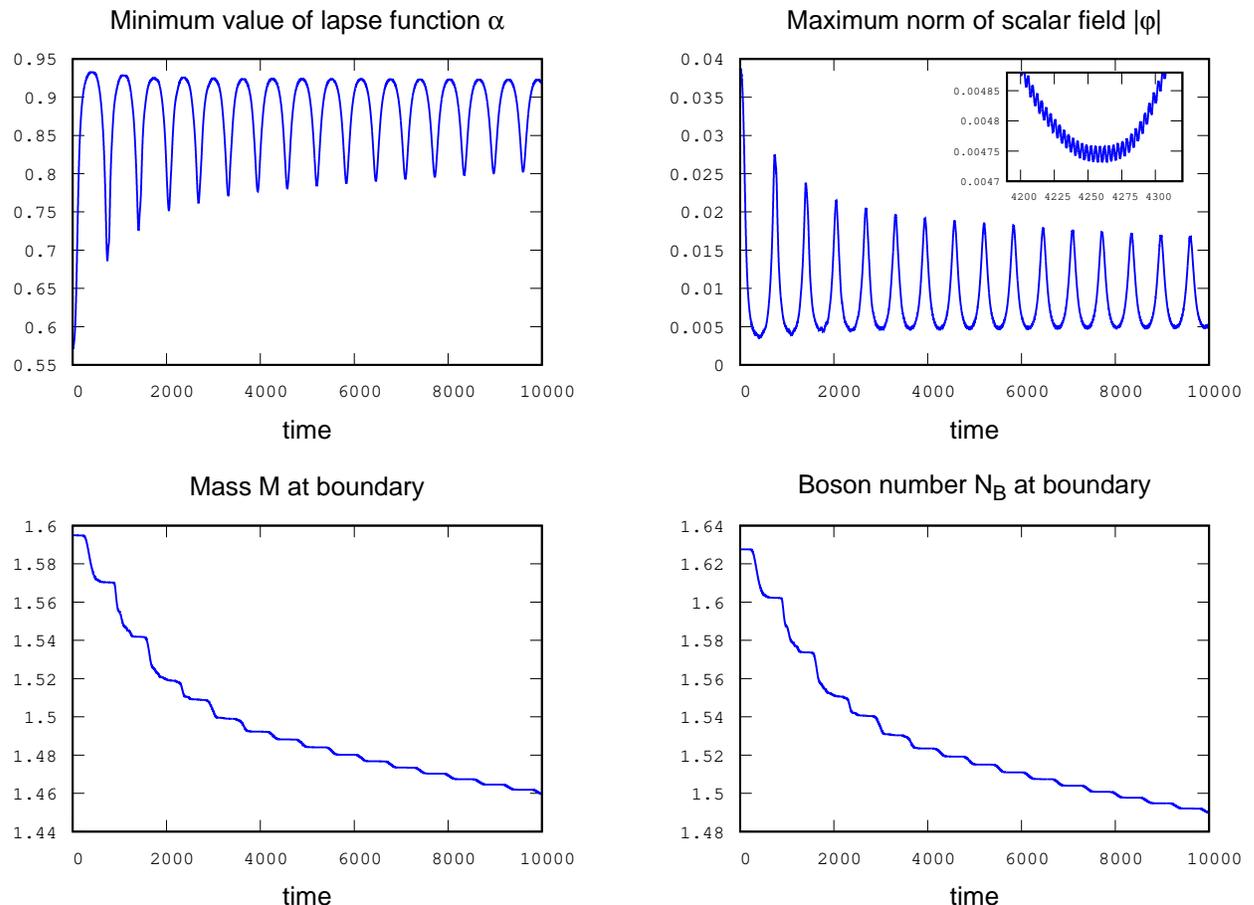
FIG. 6: Evolution in time of configuration B. This configuration migrates to the stable branch. The different panels show: Minimum of the lapse function $\alpha_{\min}$ (top-left), maximum norm of the scalar field $|\varphi|_{\max}$ (top-right), integrated mass M at the outer boundary (bottom-left), and integrated boson number N_B at the outer boundary (bottom-right). The inset to the top-right panel is a zoom to a small region of this plot to show the superposed small oscillations.

maximum of the scalar field, but located outside the star at $r = 30$. This is now an example of an unstable and unbound solution that collapses to a black hole.

Now, the 1+log slicing condition that we use has the property of "singularity avoidance", that is, the lapse collapses to zero when a black hole forms. Also, since we evolve with no shift, the collapse of the lapse is accompanied by the well-known phenomenon of "slice stretching", that is, the radial metric component grows rapidly close to the black hole horizon (see for instance [28]). All this implies that the integrated mass and boson number accumulate large errors and stop being useful quantities once the black hole forms (we are also approaching a singularity, which makes matters worse). Because of this, we have changed the quantities that we plot. We also only show the evolution up to a final time of $T = 200$, since after that the error associated with the slice stretching effect start to become very large. The four panels of Figure 8 show the minimum value of the lapse α in the top-left panel, the maximum value of the radial metric A (see equation (2)) in the top-right panel, the apparent hori-

zon position in the bottom-left panel, and the apparent horizon mass in the bottom-right panel.

Looking at the evolution of the minimum of the lapse we see that it first remains constant for some time, until the initial perturbation reaches the origin. It then shows some small oscillations, and finally, at $t \sim 100$, it starts to collapse rapidly to zero. This is an indication that a black hole has formed. The evolution of the maximum value of the radial metric A shows that it remains small and constant until $t \sim 100$, and it then starts to grow rapidly showing the typical behaviour of slice stretching. This is also indicative of the formation of a black hole.

In order to make sure that a black hole has formed, we look for the presence of an apparent horizon every 25 time steps. The bottom left panel of figure 8 shows that an apparent horizon is first found at $t \sim 117$. Its initial coordinate radius is $r \sim 3.6$, but it then grows. This growth is mostly just a coordinate effect, as the physical horizon area rapidly becomes constant. This can be seen in the bottom-right panel of the figure which shows the apparent horizon mass (which is essentially the
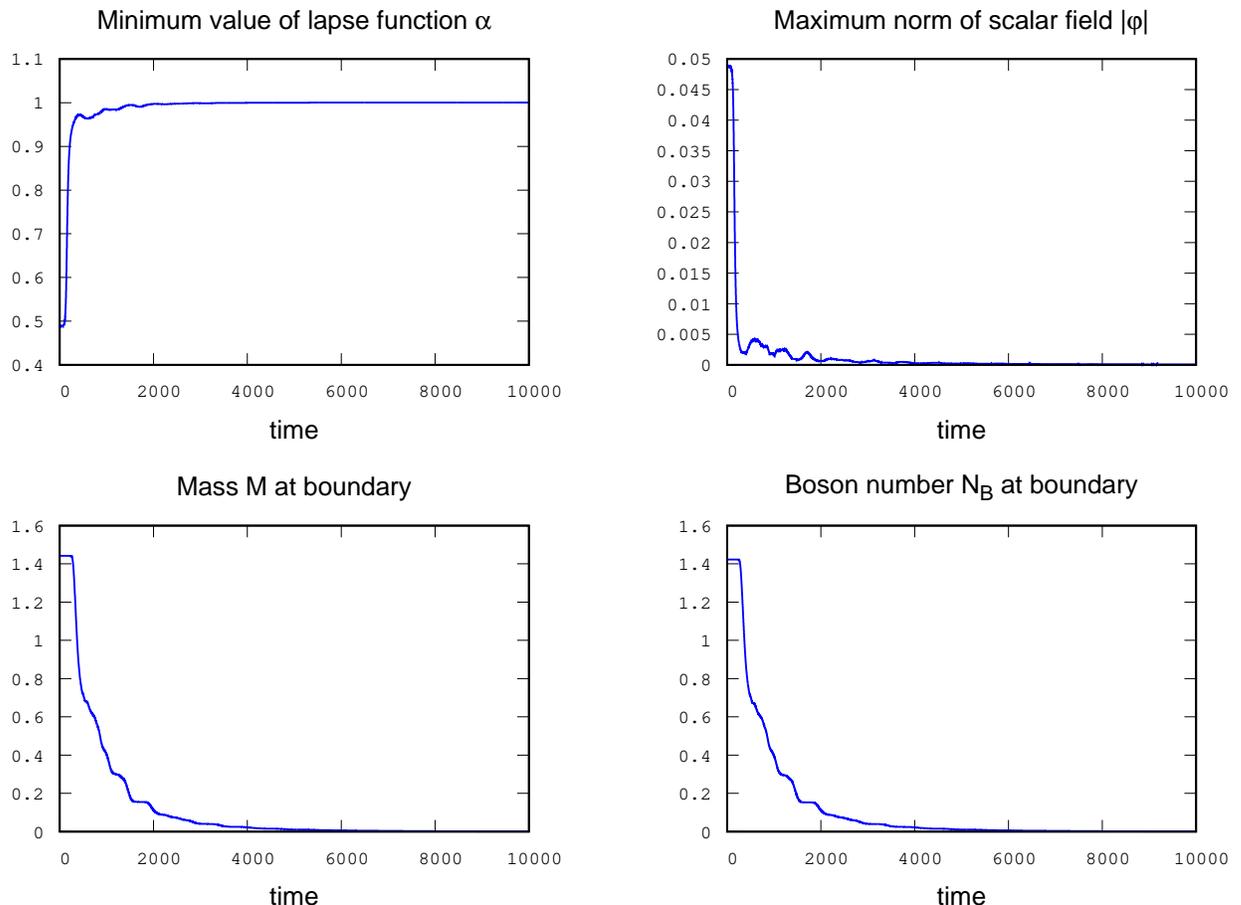
FIG. 7: Evolution in time of configuration C. This configuration explodes to infinity. The different panels show: Minimum of the lapse function $\alpha_{\min}$ (top-left), maximum norm of the scalar field $|\varphi|_{\max}$ (top-right), integrated mass M at the outer boundary (bottom-left), and integrated boson number N_B at the outer boundary (bottom-right).

square root of the area, see equation (52)). The figure shows how once a horizon forms, its mass first grows rapidly, and it then settles down to a constant value of $M_H \sim 1.443$. This is below the initial ADM mass of the configuration, which in this case is $M \sim 1.447$ (shown as a dashed horizontal line in the figure), indicating that a small amount of scalar field has been lost to infinity.

VII. CONCLUSIONS

We have performed a detailed study of the dynamical stability of the recently proposed objects dubbed ℓ-boson stars [20]. Through fully non-linear numerical simulations we have shown that, just as it happens with the $\ell = 0$ standard boson stars, for each value of ℓ the configuration of maximum mass (which seems to coincide with that of minimum binding energy) separates the parameter space into stable and unstable regions. Stable configurations react to small perturbations by oscillating and settling down to a new configuration close to the original one, though this settling down process can

be extremely slow. Unstable configurations, on the other hand, can have three quite different fates depending both on the specific type of perturbation and on the sign of the total binding energy. For most types of perturbations of unstable stars, collapse to a black hole is the most likely outcome, regardless of the sign of the binding energy. However, there are some regions of parameter space where perturbations can result either in migration to a stable configuration if the total binding energy is negative, or dispersion to infinity for a positive binding energy. As mentioned before, for both stable configurations and unstable configurations that migrate to the stable branch, the relaxation times are extremely long, and we can not rule out the possibility that those configurations will settle to some form of multi-oscillating solution such as those studied in [11].

We introduced three types of perturbations: type I is an internal perturbation to the star that changes both the total mass and boson density, type II is also an internal perturbation that preserves the boson density to linear order in small quantities, and type three is an external perturbation (scalar field falling into the boson star) that
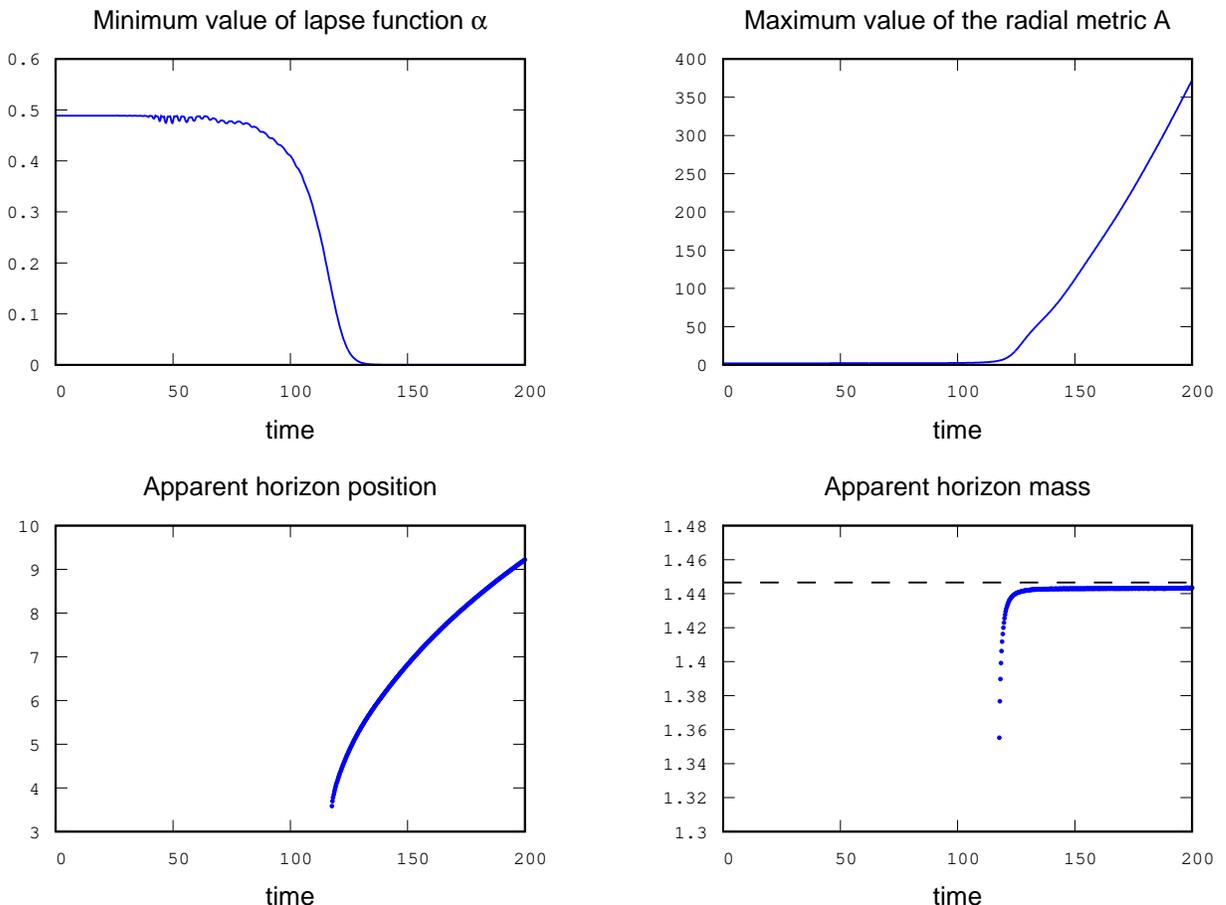
FIG. 8: Evolution in time of configuration D. This configuration collapses to a black hole. The different panels show: Minimum of the lapse function $\alpha_{\min}$ (top-left), maximum value of the radial metric $A_{\max}$ (top-right), apparent horizon position (bottom-left), and apparent horizon mass (bottom-right).

always increases the mass but can either increase or decrease the total boson number.

For unstable stars, type III perturbations always result in collapse to a black hole, which is perhaps not surprising as they always increase the total mass. Type I and II perturbations can result either in collapse to a black hole, or in migration/dispersion (depending on the sign of the binding energy). The difference between collapse and migration/dispersion seems to be related to whether the perturbation increased or decreased the total mass of the original configuration: if the mass was increased the configuration collapses, while if it was decreased it can migrate/disperse. Again, this is perhaps to be expected. However, we should mention the fact that perturbations that result in migration/dispersion for small amplitudes, result instead in collapse to a black hole if their amplitude is increased beyond a certain (still small) value, even if the sign and form of the perturbation remains the same. At this point we have not been able to find a simple physical criterion that predicts this change in behaviour.

We want to stress the role played by the ℓ parameter in our configurations: As the value of ℓ grows, one finds

more massive and compact stable objects. This fact is consistent with the intuitive idea that centrifugal effects in a rotating body oppose the gravitational pull, so that one can have more massive stable objects when compared to the non-rotating case.

It is interesting that ℓ-boson stars represent a whole new family of possible stable astrophysical objects. This encourages observational searches for compact astrophysical objects, with particular attention to features that could distinguish them from a black hole.

We close this article with two remarks. First, we would like to mention that linear perturbation theory, when applied to ℓ-boson stars, should allow one to study analytically some of the stability results that we have discussed in this work. Work in this direction is in preparation and will be presented elsewhere. Second, we stress that in this work the perturbations of the ℓ-boson star configurations have been restricted to spherical symmetry. An important problem that needs to be addresses is the extension of the stability analysis to non-spherical perturbations, either by full 3D nonlinear simulations of the Einstein-Klein-Gordon equations, or based on a lin-

earized perturbation analysis. The study of such perturbations for ℓ-boson stars should be particularly interesting, since in this case even linearized perturbations may in principle transfer energy between the different ℓ modes of the scalar field.

Acknowledgments

[1] T. Matos and L. A. Urena-Lopez, Phys. Rev. **D63**, 063506 (2001), astro-ph/0006024.

[2] H.-Y. Schive, T. Chiueh, and T. Broadhurst, Nature Phys. **10**, 496 (2014), 1406.6586.

[3] L. Hui, J. P. Ostriker, S. Tremaine, and E. Witten, Phys. Rev. **D95**, 043541 (2017), 1610.08297.

[4] A. R. Liddle and D. H. Lyth, *Cosmological Inflation and Large-Scale Structure* (Cambridge University Press, Cambridge, U.K., 2000).

[5] R. Caldwell, R. Dave, and P. J. Steinhardt, Phys.Rev.Lett. **80**, 1582 (1998), astro-ph/9708069.

[6] E. Seidel and W. Suen, Physical Review Letters **66**, 384 (1991).

[7] D. J. Kaup, Phys. Rev. **172**, 1331 (1968).

[8] R. Ruffini and S. Bonazzola, Phys. Rev. **187**, 1767 (1969).

[9] M. Colpi, S. L. Shapiro, and I. Wasserman, Phys. Rev. Lett. **57**, 2485 (1986).

[10] A. Bernal, J. Barranco, D. Alic, and C. Palenzuela, Phys.Rev. **D81**, 044031 (2010), 0908.2435.

[11] M. Choptuik, R. Masachs, and B. Way, Phys. Rev. Lett. **123**, 131101 (2019), 1904.02168.

[12] F. E. Schunck and E. W. Mielke, Class. Quantum Grav. **20**, R301 (2003), 0801.0307.

[13] S. L. Liebling and C. Palenzuela, Living Rev.Rel. **15**, 6 (2012), 1202.5809.

[14] D. F. Torres, S. Capozziello, and G. Lambiase, Phys. Rev. **D62**, 104012 (2000), astro-ph/0004064.

[15] F. S. Guzman and J. M. Rueda-Becerril, Phys. Rev. **D80**, 084023 (2009), 1009.1250.

[16] P. Amaro-Seoane, J. Barranco, A. Bernal, and L. Rezzolla, JCAP **1011**, 002 (2010), 1009.0019.

[17] K. Akiyama et al. (Event Horizon Telescope), Astrophys. J. **875**, L1 (2019).

[18] H. Olivares, Z. Younsi, C. M. Fromm, M. De Laurentis, O. Porth, Y. Mizuno, H. Falcke, M. Kramer, and L. Rezzolla (2018), 1809.08682.

[19] K. Akiyama et al. (Event Horizon Telescope), Astrophys. J. **875**, L5 (2019), 1906.11242.

[20] M. Alcubierre, J. Barranco, A. Bernal, J. C. Degollado, A. Diez-Tejedor, M. Megevand, D. Nunez, and O. Sarbach, Class. Quant. Grav. **35**, 19LT01 (2018), 1805.11488.

[21] E. W. Mielke and R. Scherzer, Phys. Rev. **D24**, 2111 (1981).

[22] H. Andreasson, J. Diff. Eq. **245**, 2243 (2008), gr-qc/0702137.

[23] I. Olabarrieta, J. F. Ventrella, M. W. Choptuik, and W. G. Unruh, Phys. Rev. **D76**, 124014 (2007), 0708.0513.

[24] T. W. Baumgarte and S. L. Shapiro, Phys. Rev. **D59**, 024007 (1998), gr-qc/9810065.

[25] M. Shibata and T. Nakamura, Phys. Rev. **D52**, 5428 (1995).

[26] J. D. Brown, Phys. Rev. **D79**, 104029 (2009), 0902.3652.

[27] M. Alcubierre and M. D. Mendez, Gen.Rel.Grav. **43**, 2769 (2011), 1010.4013.

[28] M. Alcubierre, *Introduction to* $3+1$ *Numerical Relativity* (Oxford Univ. Press, New York, 2008), ISBN 978-0-19-920567-7.

[29] C. Misner and D. Sharp, Phys. Rev. **136**, B571 (1964).

[30] M. Alcubierre, J. C. Degollado, D. Núñez, M. Ruiz, and M. Salgado, Phys. Rev. **D81**, 124018 (2010), 1003.4767.

[31] M. Ruiz, J. C. Degollado, M. Alcubierre, D. Núñez, and M. Salgado, Phys.Rev. **D86**, 104044 (2012), 1207.6142.

[32] M. Alcubierre and J. M. Torres, Class. Quant. Grav. **32**, 035006 (2015), 1407.8529.

[33] J. Balakrishna, E. Seidel, and W.-M. Suen, Phys. Rev. **D58**, 104004 (1998), gr-qc/9712064.

[34] F. Guzman, Phys.Rev. **D70**, 044033 (2004).

[35] F. Guzman, Revista Mexicana de Fisica **55**, 321 (2009).

[36] E. Seidel and W. Suen, Phys. Rev. **D42**, 384 (1990).